RADIOMETRIC CONSISTENCY INTERCOMPARISON OF GF-5, ZY-1-02D AND LANDSAT 8

Siqi Feng[1], Tao He[1], Lizhen Lei[2], Chao Lin[2]
1.School of Remote Sensing and Information Engineering, Wuhan University, No.129 Luoyu Road, Hongshan District, Wuhan, Hubei Province, 430079, China
2.Land Resource and Information Center of Guangdong Province, No. 468, Huanshi East Road, Yuexiu District, Guangzhou, Guangdong Province, 510000, China
Email: siqi_feng@whu.edu.cn; taohers@whu.edu.cn; 23864301@qq.com; 445877838@qq.com

KEY WORDS: GF-5 AHSI, ZY-1-02D AHSI, Hyperspectral remote sensing, Radiometric performance

ABSTRACT: In recent years, Chinese hyperspectral satellites represented by Gaofen-5 (GF-5) and Ziyuan-1-02D (ZY-1-02D) have been launched, which can provide abundant data sources for quantitative remote sensing applications. However, the existing hyperspectral data has narrow swaths and long revisit period. To help address large-scale and fast-changing environmental problems, it is often necessary to combine multi-source data for environment monitoring. At this time, stable and reliable radiometric quality and high consistency of multi-source data radiometric is necessary, which has become a prerequisite for the quantitative application of multi-source remote sensing. Radiometric consistency inspection based on remote sensing data has strong scalability and is less restricted by time and place. In this article, we use the column average and the overall image average to calculate the relative radiometric accuracy of the visible shortwave infrared hyperspectral cameras AHSI (the Advanced Hyperspectral Imager) carried by the GF-5 and ZY-1-02D. Due to the difference in the spectral response function of different sensors, this article has carried out band conversion on the GF-5 and ZY-1-02D data, to match the routine-calibrated Landsat 8 bands with a similar spatial resolution of 30m, and then cross-validate the radiometric consistency of these two hyperspectral sensors' apparent reflectance with the Landsat 8 data. The results show that the relative radiometric differences of GF-5 data are within 15%, and the differences of ZY-1-02D data are within 10%. Compared with the data from the 2nd to 7th bands of Landsat 8 in the adjacent time, the bias of the apparent reflectance of the GF-5 and ZY-1-02D images is within 0.015, and the root mean square error (RMSE) is less than 0.05.

1. INTRODUCTION

Since the United States successfully developed the first imaging spectrometer Airborne Imaging Spectrometer-1 (AIS-1) in 1983 (LaBaw, 1984), hyperspectral remote sensing technology has undergone nearly 40 years development and has become a cutting-edge technology in the field of passive optical remote sensing earth observation. In May 2018, the GF-5 satellite was launched in China onboard the visible shortwave infrared hyperspectral sensor AHSI. AHSI's performance indicators such as spectral resolution, the number of bands are at the international leading level(Liu et al., 2020c). In September 2019, the ZY-1-02D satellite was launched into space, which equipped with AHSI sensor providing important scientific and technological data support for hyperspectral remote sensing research. Globally, India, Italy and Japan have also sent hyperspectral sensors into space. Many sensors such as HyspIRI (Hyperspectral Infrared Imager) (Thompson et al., 2015), EnMAP (Environmental Mapping and Analysis Program) (Guanter et al., 2015) are also being planned.

Hyperspectral remote sensing technology can obtain continuous spectral images for surface, and provides richer information for quantitatively obtaining surface biochemical parameters, which widely used in vegetation detection (Riaño et al., 2002), mineral survey (Dong et al., 2020), water environmental monitoring (Giardino et al., 2020). Reliable on-orbit radiometric performance of remote sensors is the key to the quantitative application of remote sensing data. Due to the mutual constraints of remote sensing detection time resolution, spatial resolution and spectral resolution, hyperspectral data often has small image width, coarse spatial resolution and long repetition period. When conducting large-scale environmental monitoring and surveys, it is necessary to combine other multi-source data to meet the needs of applications. In this case, the radiometric consistency between multi-source data is particularly important.

The current mainstream sensor radiometric intercomparison methods can be divided into three methods: the method based on in-situ measurement data, the relative radiometric intercomparison method based on data, and the method for cross-validation from multiple remote sensing data sources. Among them, the method based on in-situ measurement data often require ground measurement or aerial aircraft to obtain the surface reflectance and atmospheric parameters at the satellite pass time, which need to know the satellite's trajectory in advance, and require a lot of time and material costs. The relative radiometric intercomparison method based on data can use

single scene data to evaluate the relative radiometric accuracy of data such as relative radiometric accuracy, information entropy, clarity, etc. It is mainly used to measure the radiometric inconsistency between different pixels of a single scene image. The method of multi-source data radiometric cross-validation is to cross-validate multi-source sensor data with similar time. This method does not require in-situ measurement, is less restricted by region and time, and does not require a lot of time and material costs.

In this article, we calculated the relative radiometric differences of the single-scene image based on the GF-5 and ZY-1-02D AHSI hyperspectral data, and used Landsat 8 data to validate the apparent reflectance radiometric consistency of GF-5 and ZY-1-02D sensors.

2. SENSOR AND RESEARCH REGION DESCRIPTION

2.1 GF-5 Advanced Hyperspectral Imager (GF-5 AHSI)

GF-5 satellite is an important scientific research satellite in Chinese Key Projects of High Resolution Earth Observation System. The satellite orbit is a 705 km sun-synchronous orbit with 7 days' revisit period (Sun et al., 2018). The AHSI camera is the main payload of the GF-5 satellite. The AHSI data have 60 km swaths width, 30 m ground resolution and 330 bands in the range of 400nm~2500nm. The spectral resolution of visible light and near-infrared (VNIR) spectrum (400nm~1000nm) is less than 5nm, and the shortwave infrared (SWIR) spectrum (1000nm~2500nm) is less than 10nm. The calibration system of the hyperspectral camera adopts the method of on-board calibration (Liu, 2018), which is used to calibrate the camera's on-orbit spectrum by combining the atmospheric profile obtained from the occultation observation.

2.2 ZY-1-02D Advanced Hyperspectral Imager (ZY-1-02D AHSI)

Like GF-5, the ZY-1-02D satellite is also equipped with a hyperspectral camera named AHSI, which can provide rich spectral information and serve quantitative remote sensing tasks (Wu et al., 2020). The AHSI boarded by ZY-1-02D has the same width and spatial resolution with the GF-5 AHSI, but different spectral setting. In the range of 400nm~2500nm, ZY-1-02D AHSI can provide 166 bands images, the spectral resolution of the VNIR bands (400nm~1000nm) is less than 10nm, and the SWIR bands (1000nm~2500nm) is less than 20nm. The ZY-1-02D AHSI calibration is completed through on-site calibration and cross-calibration (Liu et al., 2020b).

2.3 Landsat 8 Operational Land Imager (OLI)

Landsat 8 is the eighth satellite of Landsat missions, which was successful on February 11, 2013. The Landsat 8 satellite operates in a sun-synchronous orbit of 705 kilometers, and the revisit period is nearly 16 days. The Landsat 8 satellite carries two sensors: OLI and Thermal Infrared Sensor (TIRS). The image data OLI collected over a 185 km swaths with a 30 m spatial resolution for all bands except a 15 m panchromatic band (Irons et al., 2012). After verification, the absolute radiometric uncertainty of the OLI sensor is less than 5%, the apparent reflectance uncertainty is less than 3%, and the 16-day radiometric stability of the 1-8 band is better than 1% (Knight et al., 2014). The stability of the OLI is the basis for cross-validation between sensors.

2.4 Research Region

In this paper, two hyperspectral images of Guangdong Province, China are selected. The GF-5 AHSI data uses an image of Qingyuan City, Guangdong Province on February 18, 2020, in which most areas are covered by vegetation, with a small amount of urban built-up areas and rivers. The ZY-1-02D AHSI data uses an image of Zhanjiang City, Guangdong Province on December 30, 2020. Most of the image covered by bare farmland, the other are vegetation and urban built-up areas. Because the left side of the image is seriously affected by clouds, in order to avoid cloud interference, the cloud pixels were first masked before the experiment. The RGB image of the two scene images is shown in Figure 1.

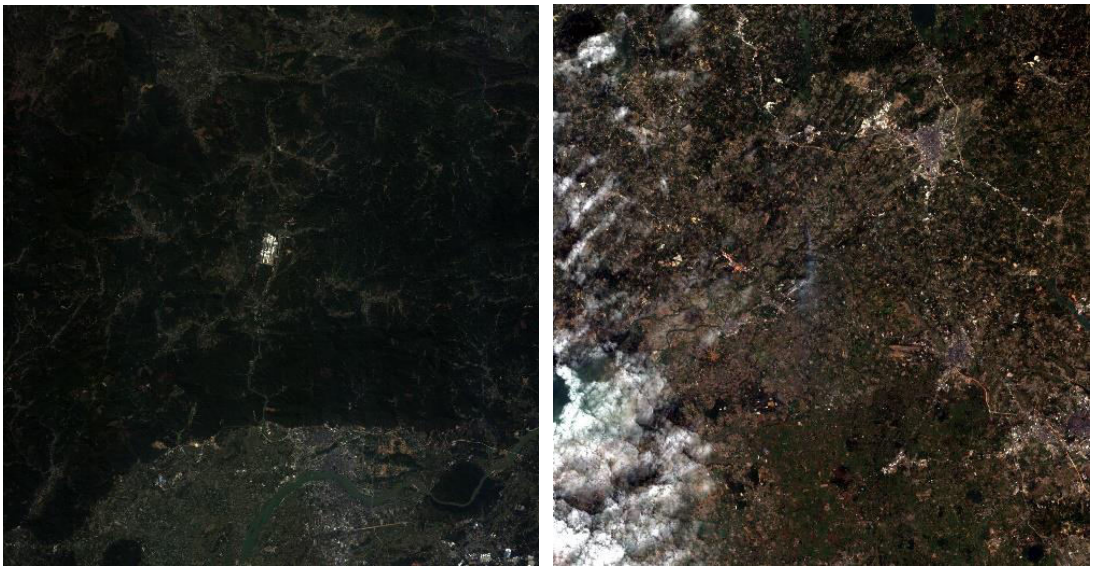

(a) (b)

Figure 1. RGB image for experiment
(a) GF-5 image on February 18, 2020, Qingyuan City, Guangdong Province, China; (b) ZY-1-02D image on December 30, 2020, Zhanjiang City, Guangdong Province, China

3. COMPARISON METHOD OF RADIOMETRIC CONSISTENCY

3.1 Relative Radiometric Difference

Due to AHSI's inconsistent spatial response, the Etalon fringes caused by the interference effect and the noise bringed by the push-broom imaging spectrometer itself (Liu et al., 2020a), make the image have the stripe noise in the column direction. In order to quantitatively evaluate the stripe noise, we use the average value of the image column and the average value of the image to evaluate the radiometric consistency of the image. This is also called the image relative radiometric calibration difference. The relative radiometric calibration difference ε_λ of the band with the center wavelength λ is:

$$\varepsilon_\lambda = \frac{1}{\overline{DN}} \frac{\sum_{j=1}^{n} |DN(j) - \overline{DN}|}{n} \quad (1)$$

$\overline{DN}$ is the average value of the band image with the center wavelength λ, n is the number of image columns, and $DN(j)$ represents the average value of the pixel in the jth row of the image.

3.2 Cross-validation of Radiometric Consistency Method

The cross-validation method of radiometric consistency is based on two suppose that the radiometric energy of the same target obtained by two sensors at similar time under similar observation geometric conditions is equal in the same waveband, and the target's spectral characteristic is not changed. In the actual application process, there are differences in the spectral response function between different sensors. Therefore, before performing cross-validation of radiometric consistency, it is necessary to perform spectral matching on different sensors to correct the systematic error caused by the difference of the spectral response function.

3.2.1 Spectral Match

The apparent radiance obtained by the sensor can be expressed as:

$$L_i = \frac{\int L(\lambda) S_i(\lambda) d\lambda}{\int S_i(\lambda) d\lambda} \tag{2}$$

L_i represents the apparent radiance obtained by the sensor in the i band. $L(\lambda)$represents the apparent radiance at λ wavelength, $S_i(\lambda)$ represents the i band spectral response function of sensor at λ wavelength.When the center wavelength and spectral resolution of the two sensors are similar, assuming that $L(\lambda)$ has a small change in the wavelength range, the influence of this little difference can be ignored. Thus, the spectral matching correction factor k of the two sensors can be obtained:

$$k = L_{i,A}/L_{j,B} \tag{3}$$

$L_{i,A}$ represents the apparent radiance obtained by the sensor A in the i band, $L_{j,B}$ represents the apparent radiance obtained by the sensor B in the i band.When it comes to hyperspectral sensors and multispectral sensors, due to the large difference in spectral resolution, it may not meet the assumption that the small difference of apparent radiance. Therefore, the hyperspectral data can be integrated according to the center wavelength and the spectral response function of multi-spectral data band to calculate the spectral conversion correction factor.

3.2.2 Radiometric Calibration

The pixel data in the Level 1 remote sensing data is a digital number (DN) with no physical meaning. The image needs to be radiometric calibrated to convert the DN into apparent radiance $L(\lambda)$. For GF-5 AHSI and ZY-1-02D AHSI data, the radiometric calibration formula is:

$$L = DN * gains + offset \tag{4}$$

According to different imaging observation geometry and imaging time, the apparent reflectance ρ^* can be calculated from the apparent radiance $L(\lambda)$.

$$\rho^*(\theta_s, \theta_v) = \frac{\pi * L(\theta_s, \theta_v)}{E_0 * \cos(\theta_s)} \tag{5}$$

θ_s represents the solar zenith angle, θ_v represents the view zenith angle, E_0 represents the irradiance of the sun at the top of atmosphere, which can be calculated from the solar spectrum and the distance between the sun and the earth.

4. RESULTS

4.1 Relative Radiometric Difference of the Single-scene Image

The relative radiometric difference can be used to quantitatively measure the strength of image stripe noise. In order to reduce the impact of surface differences on the results and to ensure that calculation covers the entire image coverage area, the part of the image with no clouds and relatively uniform ground objects distribution is intercepted

to calculate the relative radiometric difference. According to the characteristics of the AHSI image, the column average is used to evaluate the image stripe noise. The relative radiometric differences of GF-5 AHSI (Figure 2(a)) and ZY-1-02D AHSI (Figure 2(b)) in each band are plotted. Because AHSI does not provide data in some of the water vapor absorption bands and the image signal-to-noise ratio of some bands near the water vapor absorption bands is too low to provide effective information, in the experiment, the bands which center wavelength is between 1350-1500nm, 1800-2000nm after 2450nm were excluded.

The AHSI sensor is equipped with two spectrometer: VNIR and SWIR. The comparison of the two spectrometer images shows that the relative radiometric differences of the sensor in the VNIR bands is relatively small, and the error in the SWIR bands is relatively large. In the VNIR bands, the relative radiometric accuracy of ZY-1-02D AHSI is better than that of GF-5 AHSI. In the shortwave infrared 1500-1800nm and 2000-2500nm bands, the relative radiometric accuracy of the two AHSI sensors are similar.

In the bands near the water vapor absorption bands of 1400nm, 1900nm, and 2500nm, due to the influence of water vapor absorption, the apparent radiometric energy received by the sensor is weak, and the relative radiometric differences are large. The relative radiometric differences in the visible light bands shows an increase with the increase of the wavelength, which may be caused by the longer wavelength in the visible light bands, the stronger heterogeneity of the apparent reflectance of the surface.

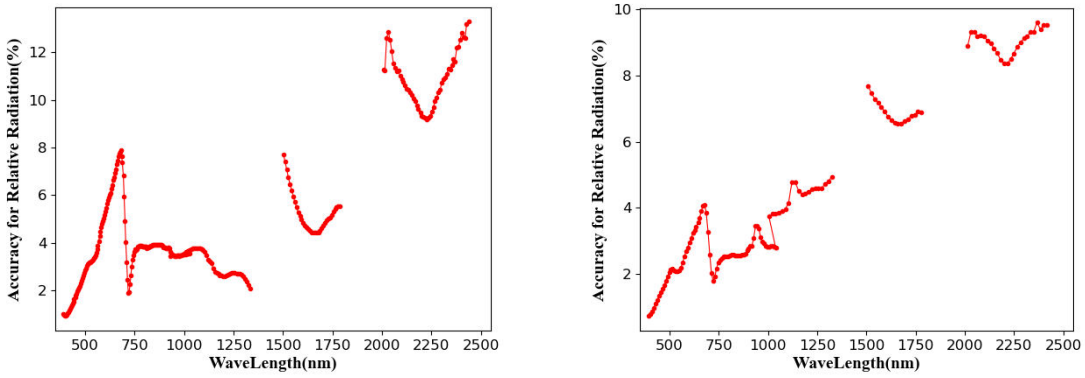

(a) GF-5 AHSI (b) ZY-1-02D AHSI

Figure 2. The relative radiometric differences of the experimental image

Table 1. The average relative radiometric differences of VNIR and SWIR bands

spectrometer	wavelength(nm)	GF-5 AHSI average relative radiometric differences	ZY-1-02D AHSI average relative radiometric differences
VNIR	400-750	3.8%	2.3%
	750-1030	3.7%	2.8%
SWIR	1000-1350	3.0%	4.4%
	1500-1800	5.4%	6.9%
	2000-2450	11.0%	9.1%

4.2 Cross-validation of Apparent Reflectance Radiometric Consistency

In order to cross-validate the apparent reflectance radiometric consistency of the GF5, ZY-1-02D AHSI with the Landsat 8 similar acquisition time data, the spectral matching method described in section 3.2 is used to perform to

match the hyperspectral data to Landsat8. Tables 2 and 3 show the image information of the GF5, ZY-1-02D AHSI images and Landsat 8 data at similar acquisition time.

Table 2. GF5 and Landsat8 image information

	GF5 AHSI	Landsat 8 OLI
Acquisition time (UTC+8)	2020-02-18 13:36	2020-02-18 10:52
Solar zenith angle	38.01°	43.76°
View zenith angle	0.075°	

Table 3. ZY-1-02D and Landsat8 image information

	ZY-1-02D AHSI	Landsat 8 OLI
Acquisition time (UTC+8)	2020-12-30 03:33	2021-01-01 11:05
Solar zenith angle	47.63°	50.61°
View zenith angle	0.359°	

Figure 3 and 4 show the comparison of the apparent reflectance of the randomly selected large homogeneous non-cloud AHSI pixels with Landsat8 pixels in the same location. The absolute deviation of the apparent reflectance of the GF-5 and ZY-1-02D AHSI in the 2nd to 7th bands of Landsat8 is within 0.015. Compared with the infrared bands, the apparent reflectance in the visible light bands is lower and more concentrated, the relative root mean square error is also smaller, which is less than 0.02. In Landsat8's 2nd to 4th band (visible light bands), the deviation and RMSE of GF-5 data are smaller than those of ZY-1-02D, and the apparent reflectance consistency is better than that of ZY-1-02D. In the 5th band of Landsat8 which central wavelength is 865nm, the apparent reflectance of ZY-1-02D sensor is more consistent with Landsat8; in the 6th and 7th shortwave infrared bands of Landsat8, the apparent reflectance consistency of the two sensors is similar.

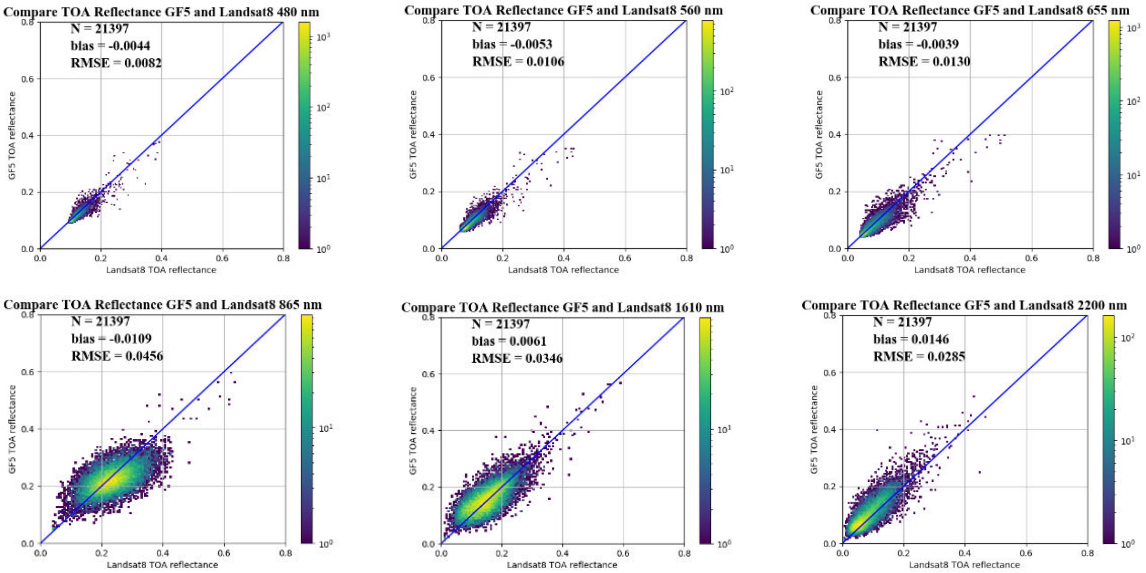

Figure 3. Scatter plot of GF-5 AHSI apparent reflectance after spectral matched and Landsat8 2-7 band apparent reflectance

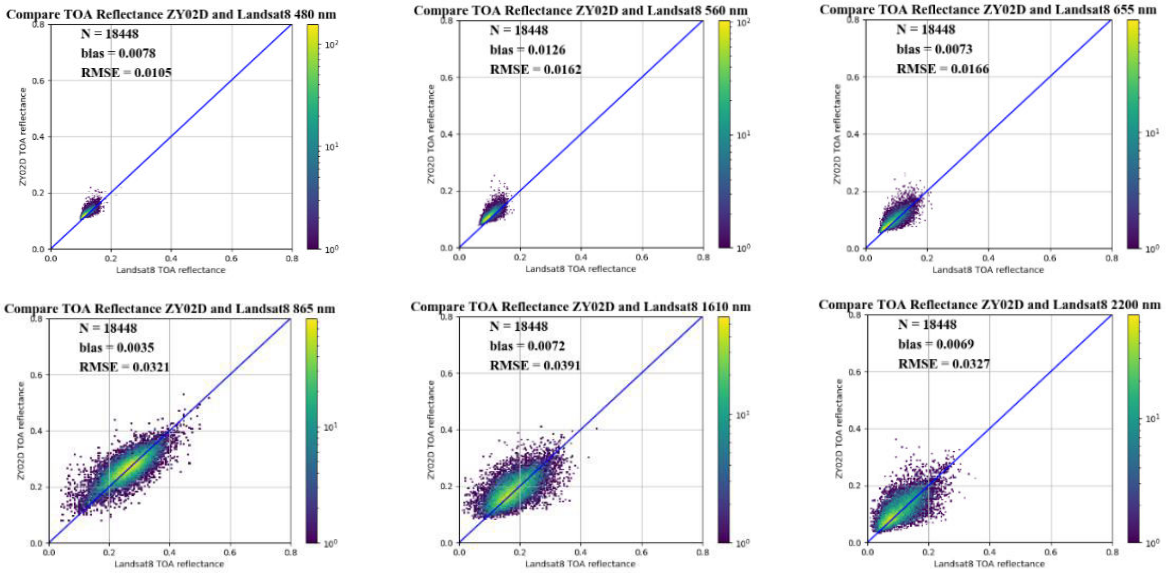

Figure 4. Scatter plot of ZY-1-02D AHSI apparent reflectance after spectral matched and Landsat8 2-7 band apparent reflectance

5. CONCLUSION AND DISCUSSION

In this paper, the column average method was used to calculate the relative radiation difference of the two images of GF5 and ZY-1-02D AHSI, and to quantify the relative radiometric difference of each bands. The results show that the relative radiometric differences of the two images in the VNIR bands is less than that in the SWIR bands. Excluding the bands near the water vapor absorption bands, the relative radiometric error of most bands is less than 10%. The results of the relative radiometric differences show two phenomena: one is the relative radiometric error near the water vapor absorption bands is relatively large, the other is the error in the visible light bands shows a trend of increasing with the wavelength. The possible causes of the two phenomena had been analyzed. This paper used Landsat8 data to cross-validate the apparent reflectance of AHSI sensors. The deviation of the apparent reflectance was calculated to cross-validate the radiometric consistency of these two AHSI sensors with Landsat 8 OLI, which was less than 0.015, most of them are less than 0.01. The VNIR bands' apparent reflectance accuracy of GF-5 AHSI is slightly better than that of the SWIR bands. For ZY-1-02D AHSI, the accuracy is relatively similar, all around 0.07.

This paper proved that after the GF-5 and ZY-1-02D AHSI data to match the Landsat8 bands, they have good radiometric consistency with Landsat8 data on a larger spectral width. The validation of the radiometric quality of each band on the narrower spectral width needs supplementary validation. Since the view zenith angle of GF-5 and ZY-1-02D AHSI data is close to 0, which is similar to Landsat 8, and Landsat 8 data with similar acquisition time had been selected, so this paper didn't consider the influence of BRDF effect on cross-validation. If the sensor's view zenith angle deviates from 0, or there is a large solar zenith angle deviation between the cross-validation data, the BRDF effect needs to be taken into consideration. In addition, the radiometric stability of the sensor will be affected by various factors, and the performance of the sensor may decline over time. Monitoring whether the performance of the data has any changes over a long period of time, it is the key to ensure the performance of the data. In the future, it is necessary to continuously detect the performance of the sensor over a long period of time. And it is necessary to validate the sensor performance with in-situ measurements.

ACKNOWLEDGEMENTS

We thank the financial and data support from the Land Resource and Information Center of Guangdong Province for the GF 5 and ZY-1-02D hyperspectral satellite data, and we would also like to thank for the Landsat data distributed by the USGS.

REFERENCES

Dong, X., F., Gan, F., P., Li, N., Yan, B., K., Zhang, L., Zhao, J., Q., Yu, J., C., Liu, R., Y. & Ma, Y., N., 2020. Fine mineral identification of GF-5 hyperspectral image. Journal of Remote Sensing, 24 (4), pp.454-464.

Giardino, C., et al., 2020. First Evaluation of PRISMA Level 1 Data for Water Applications. Sensors, 20(16), pp. 4553.

Irons, J., R., Dwyer, J., L. & Barsi, J., A., 2012. The next Landsat satellite: The Landsat Data Continuity Mission. Remote Sensing of Environment, 122, pp. 11-21.

Knight, E. & Kvaran, G., 2014. Landsat-8 Operational Land Imager Design, Characterization and Performance. Remote Sensing, 6(11), pp. 10286-10305.

LaBaw, C., 1984. Airborne Imaging Spectrometer: An Advanced Concept Instrument. In: 27th Annual Technical Symposium.

Liu, Y., N., 2018. Visible-shortwave Infrared Hyperspectral Imager of GF-5 Satellite Spacecraft Recovery & Remote Sensing, 39(3), pp. 25-28.

Liu, Y., N., Sun, D., X., Cao, K., Q., Liu, S., F., Chai, M., Y., Liang, J. & Yuan, J., 2020a. Evaluation of GF-5 AHSI on-orbit instrument radiometric performance. Journal of Remote Sensing, 24 (4), pp.352-359.

Liu, Y., N., Sun, D., X., Han, B., Zhu, H., J., Liu, S., F. & Yuan, J., 2020b. Development of Advanced Visible and Short-wave Infrared Hyperspectral Imager Onboard ZY-1-02D Satellite. Spacecraft Engineering, 2020b, 29(6), pp.85-92.

Liu, Y., N., Sun, D., X., Hu, X., N., Liu, S., F., Cao, K., Q., Chai, M., Y., Liao, Q., J., Zuo, Z., Q., Hao, Z., Y. & Duan, W., B., 2020c. Development of visible and short-wave infrared hyperspectral imager onboard GF-5 satellite. Journal of Remote Sensing, 24 (4), pp.333-344.

Riaño, D., Chuvieco, E., Ustin, S., Zomer, R., Dennison, P., Roberts, D. & Salas, J., 2002. Assessment of vegetation regeneration after fire through multitemporal analysis of AVIRIS images in the Santa Monica Mountains. Remote Sensing of Environment, 79(1), pp. 60-71.

Sun, Y., Jiang, G., Yunduan, L., I., Yang, Y., Dai, H., Jun, H., E., Qinghao, Y., E., Cao, Q., Dong, C. & Zhao, S., 2018. GF-5 Satellite: Overview and Application Prospects. Spacecraft Recovery & Remote Sensing, 39(3), pp. 1-13.

Thompson, D., R., Gao, B., C., Green, R., O., Roberts, D., A., Dennison, P., E. & Lundeen, S., R., 2015. Atmospheric correction for global mapping spectroscopy: ATREM advances for the HyspIRI preparatory campaign. Remote Sensing of Environment, 167, pp. 64-77.

Wu, X., D., Wang, J., Zhao, Y., Zhang, H., Y., Wang, X., H., Wei, X., Zhang, J., Y. & Jia, J., Data Balance Analysis and Design of ZY-1-02D Satellite. Spacecraft Engineering 29 (6), pp. 51-59.